Confined crystal melting in edgeless poly (L-lactic acid) crystalsomes

Mark C. Staub,[†] Ruipeng Li,[‡] Masafumi Fukuto,[‡] Christopher Y. Li[†]*

[†]Department of Materials Science and Engineering, Drexel University, Philadelphia, Pennsylvania, 19104 United States

[‡]National Synchrotron Light Source II, Brookhaven National Laboratory, Upton, New York 11973, United States

KEYWORDS: Polymer crystallization, polymer single crystals, crystalsomes, crystal melting

ABSTRACT Polymer single crystals tend to be quasi two-dimensional (2D) lamellae and their small lateral surfaces are the starting points of lamella melting and thickening. However, the recently discovered crystalsomes, which are defined for hollow single crystal-like spherical shells, are edgeless, self-confined, and incommensurate with translational symmetry. This work concerns the structure and melting behavior of these edgeless crystalsomes. Poly (L-lactic acid) crystalsomes were grown using a miniemulsion solution crystallization method. Differential scanning calorimetry and *in-situ* wide-angle X-ray diffraction were used to follow the structural evolution of the crystalsomes upon heating. Our results demonstrated that the structure and melting behavior of crystalsomes are curvature-dependent and significantly different from their flat crystal counterpart.

A dominant morphological feature of polymer crystals is their quasi two-dimensional (2D) shape. Since polymer chains fold back and forth in this 2D shape, growth along the normal of the top and bottom fold surfaces is typically prohibited, leading to 2D polymer lamellae with a high aspect ratio (lateral size over thickness) of hundreds to tens of thousands.[1-2] This 2D feature is fundamental in understanding the thermodynamics of polymer crystallization because the crystal growth can be viewed as the advancement of a lamella's lateral surface into a polymer melt or solution. Due to the small dimension of the lateral surface compared with the fold surface, they are often omitted in a Gibbs-Thomson type of crystallization/melting analysis.[1, 3] However, because of the high surface energy and chain mobility, the melting/thickening process of a lamella often starts from its edge,[4-5] which has been observed in annealing experiments in poly(ethylene),[6-7] poly(ethylene oxide),[8-9] and poly(L-lactic acid) (PLLA)[10].

An interesting question therefore arises: how does an edgeless lamellar crystal melt? To create an edgeless lamellar crystal, we consider the recently discovered spherical crystalsomes, which are single crystal-like hollow crystalline shells.[11-16] Due to its spherical shape, no exposed crystalline lateral surfaces exist in a closed crystalsome. Two types of approaches have been used to grow this unique structure. First, homopolymer and block copolymer crystalsomes were obtained using a miniemulsion crystallization method.[11-13] Second, molecular bottlebrushes with crystalline side chains were used to spontaneously form hollow crystalsomes.[14] The present study concerns the structure and meting behavior of such crystalsomes. We shall focus on two aspects of the crystalsomes. First, crystalsomes are edgeless and self-confined; therefore, they do not have mobile lateral surfaces to initiate the crystal melting process. Second, crystalsomes belong to a class of "shape-translational symmetry incommensurate crystals" (SSIC),[17] where, due to the intrinsic non-flat shape, translational symmetry is broken. Similar examples are banded spherulites,[7, 18] helicoidal,[19] scrolled,[20-22] bowl-shaped single crystals,[23] etc. SSICs are defect-rich, which significantly affects their structure and melting behavior.

The previously reported PLLA homopolymer crystalsomes were used in the present study as the model system. PLLA exhibits intriguing and diverse melting behavior.[24-25] From bulk crystallization, profound behaviors, such as multiple melting, broad endotherms, and phase transitions just before the final melting peak, have been observed in differential scanning calorimetry (DSC) experiments.[26-33] Our results in this work demonstrated that the confined melting of the edgeless PLLA crystalsomes is significantly different from the melting behavior of a conventional polymer lamellae. Curvature-dependent structural evolution upon heating was observed in crystalsomes with different sizes.

Figure 1a shows a schematic of the miniemulsion crystallization method to form PLLA crystalsomes, and the detailed experimental procedure can be found in the supporting information. In this process, slow crystallization in the confined emulsion droplet allowed for the formation of lamellar crystals guided by the curved liquid/liquid interface, leading to the single crystal-like crystalsomes with the polymer chains perpendicular to the crystalsome surface.[11] **Figure 1b** is a TEM micrograph of a typical crystalsome grown at 90°C for 48 hr, with the insets showing the corresponding selected area electron diffraction (SAED) pattern (bottom inset) and a scanning electron microscopy (SEM) image (top inset). The spherical

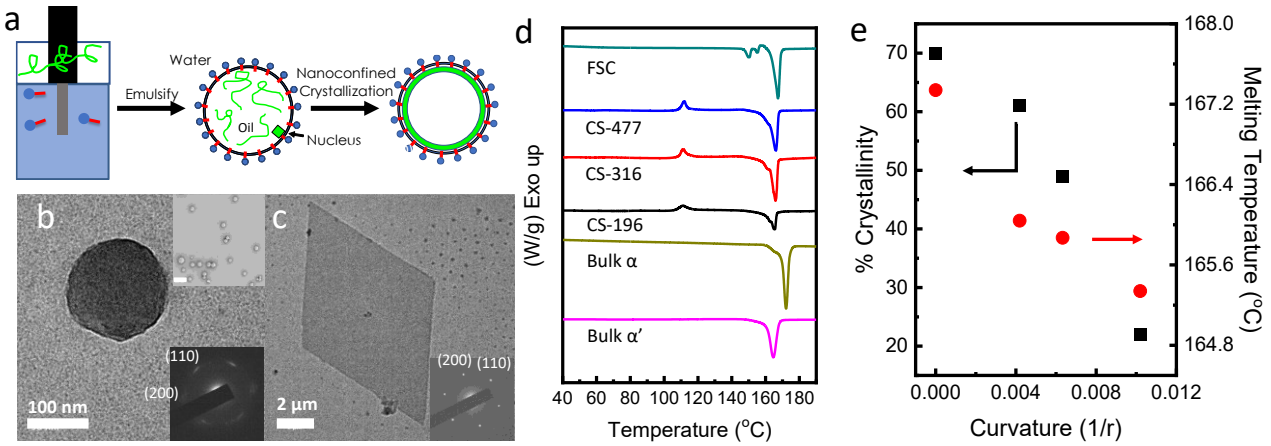

Figure 1. Formation process and thermal properties of PLLA crystalsomes. (a) Schematic of miniemulsion solution crystallization, (b) A TEM micrograph of a PLLA crystalsome grown at 90 °C with insets showing a SAED pattern of the crystalsome (bottom) and an SEM micrograph of PLLA crystalsomes (top, scale bar 1 μm). (c) TEM of a PLLA single crystal grown using a self-seeding technique (see supporting information) with inset showing the SAED pattern. (d) First heating DSC thermograms of PLLA FSCs, crystalsomes with different sizes, and α and α` bulk phases (from top to bottom). (e) Plot of percent crystallinity (black squares) and T_m (red circles) versus the degree of curvature.

morphology of the crystalsome is evident, in stark contrast to the flat, lozenge shaped PLLA lamellae grown in solution (**Figure 1c**). SAED patterns of the PLLA crystalsomes and flat single crystals (FSC) exhibited the same symmetry (**Figure 1b,c** insets) as α phase PLLA single crystals.[34-35] However, the FSCs showed sharp diffraction spots and arc-shaped diffractions were observed in PLLA crystalsomes; the latter was attributed to the continuous lattice splaying in the curved space in the crystalsomes.[11] Wide-angle X-ray diffraction (WAXD) was further used to evaluate the structure of FSCs versus the crystalsomes. The increased peak width suggested greater structural disorder incorporated into the crystalsomes due to their curved space.[11] In this work, DSC along with *in-situ* heating synchrotron WAXD were utilized to study the melting of crystalsomes versus PLLA FSCs. To examine the size-dependency, a centrifugation procedure (detailed in the supporting information) was used to separate the as-formed crystalsomes into three batches with different average diameters of 477 nm, 316 nm, and 196 nm crystalsomes, respectively (denoted as CS-477, CS-316, and CS-196), and the crystalsome sizes were confirmed using dynamic light scattering (Figure S2).

Figure 1d shows the DSC thermograms of different forms of PLLA crystals, including the flat PLLA single crystals obtained from solution crystallization at 25 °C, the crystalsomes with three different sizes, and bulk PLLA having an α or α` structure. Note that the growth condition for PLLA FSCs was chosen so that a relatively large quantity of FSCs can be obtained for bulk analysis and the FSC thickness (~11.8 nm, Figure S3) is similar to that of the PLLA crystalsome (~11.0 nm) as previously reported.[11] A 10 °C/min heating rate was applied, and all the curves shown were from first heating experiments The FSCs curve shows the prominent multiple melting observed where there are two small endotherms prior to a small recrystallization exotherm followed by the large endotherm of the final melting. The crystallinity (X_c) and melting temperature (T_m) was plotted against curvature in **Figure 1e**. The curvature of a PLLA crystalsome was define as $\kappa = \frac{1}{r}$, where κ is the curvature and r is the crystalsome radius. The radius of an FSC is considered infinite, and its curvature is zero. The crystallinity of the FSCs, using a ΔH_f of 91 J/g for a 100% crystalline sample, is 70% and the T_m is 167.3 °C.[36]

There are several differences observed in the DSC heating curve of CS-477 (blue curve in **Figure 1d**) compared with the FSCs. First, there is a clear recrystallization peak at ~110 °C. This can be ascribed to the defect-rich nature of crystalsomes as evidenced by their lower crystallinity compared with FSCs, which suggests that the crystals have more "room" to improve local chain packing. Second, multiple melting is absent in the melt region, and only a slight shoulder is observed prior to the main melting. The X_c is 61% and T_m is 166 °C, both are lower than that of FSCs. Note that for crystalsomes, the X_c was calculated by subtracting the enthalpy of the recrystallization peak from that of the melting enthalpy so the result reflects the initial crystalsome structure without annealing effects. As we move to the two smaller crystalsome curves, the same major features (*e.g.* recrystallization and single melting peak with a slight pre-melting shoulder) are seen as in the case of CS-477, while quantitative changes in X_c and T_m can be observed. For CS-316, the X_c and T_m are 49% and 165.9 °C, and CS-196 has an X_c and T_m of 22% and 165.3 °C, respectively. The decrease in the X_c confirms that as the curvature increases, greater structural disorder is incorporated in the crystalsomes, which is generally consistent with X_c calculations from WAXD.[11] The decrease of T_m with increasing crystalsome curvature indicates the smallest crystalsomes (greatest curvature) have the least stable crystal structure.

To put these results into the context of the intensely studied bulk PLLA, two bulk samples were prepared by quenching the samples to either 150 °C or 80 °C and crystallized for 10 hr to produce bulk PLLA α and α` phases, respectively.[31-32] The first heating curves of these samples are shown at the bottom of **Figure 1d**. A single melting endotherm is observed with the α phase curve having a slight shoulder prior to melting. The T_m

of the α and α` curves are 172.0 °C and 164.4 °C respectively. The DSC experiments therefore confirms that metastability of different PLLA crystals follows the order of α phase bulk > α phase FSC > α phase crystalsome > α` bulk with the crystalsome α phase scaling with size where the smallest crystalsomes are least stable.

The DSC results show clear differences in the melting behavior of spherical crystalsomes compared with FSCs. In order to better understand the evolution of chain packing during the melting process, *in-situ* heating WAXD was utilized. The samples analyzed were the PLLA FSCs, CS-316, and CS-196. **Figure 2a** shows the room temperature WAXD profiles of the three samples. The results are consistent with previously reported data where all profiles are α phase PLLA.[11] The (110/200) peak has the greatest intensity in the WAXD profiles and will therefore be used to follow the structural changes as a function of temperature. **Figure 2b-d** shows the *in-situ* heating WAXD profiles of the (110/200) peak for

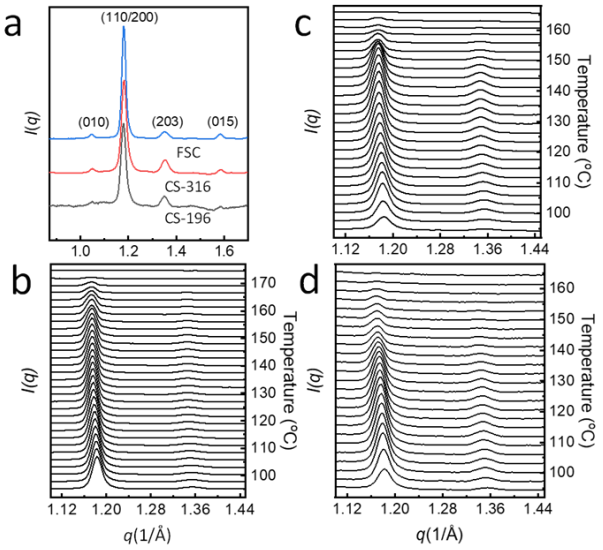

Figure 2. Structural evolution of PLLA FSC and crystalsomes upon heating. (a) Room temperature WAXD profiles of PLLA FSC (blue), CS-316 (red), and CS-196 (black). (b-d) *In-situ* heating WAXD profiles of PLLA FSC (b), CS-316 (c), and CS-196 (c).

FSCs, CS-316, and CS-196. All three samples show a clear peak shift to lower q values as a function of temperature, which can be attributed to thermal expansion when heated. Note that when the crystalsomes approach the melt region there is no sudden shift to a higher q value. It has been documented in literature that when the α` phase is heated there is an abrupt shift to higher q right before the melt region.[32] The absence of this abrupt and appreciable q shift at higher temperature in the crystalsomes further confirms that α` phase is absent in all three samples. This indicates, as also shown by DSC, the lamellar reorganization and melting mechanism in the crystalsomes is distinct from the α` to α transition.

In order to quantitatively assess the WAXD profiles the (110/200) peaks were fit with a Lorentzian function using Origin Pro to obtain the peak maximum and full width at half maximum (FWHM). The d-spacing and crystallite size (coherence length, D_{hkl}, where the subscript *hkl* denotes the miller index of the crystallographic planes corresponding to the reflection peak) were calculated, the later using the Scherrer equation ($D_{hkl} = 2\pi/FWHM$).[37] **Figures 3a-c** show plots of d-spacing (black square) and crystallite size (red circles) as a function of temperature from 100 °C through the crystals respective melting temperatures. The first heating DSC curve of each sample is included (light blue) to correlate the WAXD and DSC results as will be discussed below.

Figure 3a shows the d-spacing and crystallite size change for the FSCs. Below ~144 °C, the increase in d-spacing is linear and the slope 6.8 x 10^{-4} Å/°C; which can be considered as the coefficient of thermal expansion (CTE) of (110)/(200) planes. The value is slightly higher than bulk PLLA previously reported.[32] Once the temperature of the first small endotherm from DSC is reached (144 °C), the CTE decreases to 4.6 x 10^{-4} Å/°C, and maintains this value until complete melting of the crystal. Turning to the crystallite size, prior to the pre-melting observed in DSC, the crystallite size increases from 335 to 357 Å. Just before 140 °C and the first small endotherm, a sudden sharp increase is observed to 365 Å at 144 °C, followed by a steady decrease through the entire melt region.

For CS-316 (**Figure 3b**), the d-spacing trend is similar to that of FSCs, and there is a constant CTE of 7.8 x 10^{-4} Å/°C from 100 °C until the pre-melt region (~144 °C) is reached followed by a decrease in CTE to 5.8 x 10^{-4} Å/°C through the melt region. **Figure 3d** shows an overlay plot of the d-spacing of all three samples, and it is seen that the d-spacing of CS-316 is similar to that of the FSCs in the entire temperature range. A similar increase in crystallite size is observed up to the pre-melt temperature, but then a sharp increase in slope is observed until the main endotherm is reached. Compared with the FSCs, the crystallite size upturn region in CS-316 upshifted to 144–161 °C. For CS-196, the trends are very different. The d-spacing of CS-196 shows a fairly linear CTE of 8.0 x 10^{-4} Å/°C up to the pre-melting temperature, which is also ~144 °C. Then a sudden increase in CTE to1.5 x 10^{-3} Å/°C is observed through the melt region (144–154 °C) before decreasing to 9.9 x 10^{-4} Å/°C. The overlay plot of d-spacings in **Figure 3d** also identifies that the d-spacing of the small crystalsome is greater than that of the FSCs and large crystalsomes. The crystallite size shows a very different trend where the size quickly reaches ~260 Å and then slightly increases to just over 280 Å before melting.

The above DSC and WAXD results are summarized as four major findings that are associated with the two main characteristics of crystalsomes: the absence of lateral surface (edgeless crystals) and the spherical shape, detailed as following.

1) ***Multiple vs. single DSC melting endotherms***. FSCs show multiple melting peaks while single melting peaks with a shoulder were observed in crystalsome samples. The multiple melting peaks in PLLA FSCs can be attributed to the annealing/thickening of the FSCs upon heating. As previously discussed, polymer chains near the lateral surface are more mobile and prone to thickening upon heating; continuous thickening/melting leads to the observed multiple melting peaks. The lack of lateral surface in a crystalsome indicates that mobile chains on a crystal lateral surface are absent. Furthermore, the closed crystalsome morphology also produces tighter chain packing and the crystals are self-confined. Both factors would lead to slower chain reorganization in crystalsomes. Note that for crystalsome melting, when Gibbs-Thomson equation is

used, the surface energy could be different from the conventional value because crystalsomes are hollow. Elastic bending energy[38] and distorted lattice dimension could also affect the analysis.

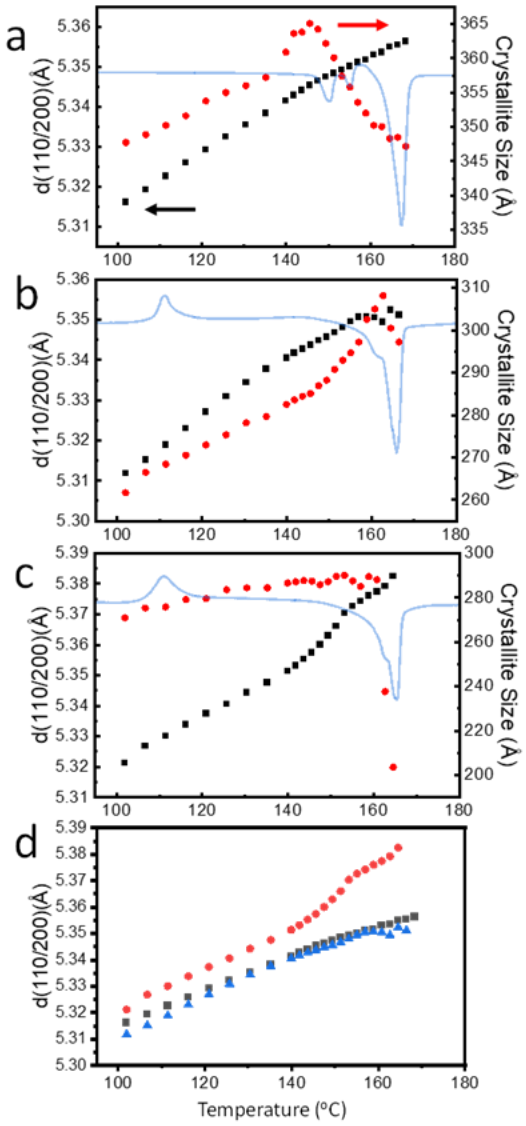

Figure 3. Plot of crystallite size (red circles) and d-spacing of (110/200) plane (black squares) as a function of temperature for single crystal (a), CS-316 (b), and CS-196 (c) overlaid on the first heating DSC scan of the respective samples. Overlay of single crystal (black squares), CS-316 (blue triangle), and CS-196 (red circles) d-spacing of (110/200) plane (d).

2) ***Curvature dependent crystallinity and d-spacing***. DSC results showed that the crystallinity decreases and the (110)/(200) d-spacing increases in the crystalsomes as the curvature κ increases (**Figure 1e**). CS-196 shows slightly greater d-spacing than the FSC and CS-316 in the entire temperature range. The curvature dependent crystallinity and d-spacing can be attributed to the crystalsome shape and translational symmetry incommensurability. Since PLLA chains are perpendicular to the crystalsome surface, in crystalsomes, the PLLA stems must splay in order to accommodate the curved space, as shown in **Figure 4**. This splay can be quantified by calculating a relative "strain" in the crystalsome from the inner to outer shell layers by using $\varepsilon = \frac{2l}{2r-l}$, where l is the crystal thickness (11nm as previously reported) and r is the radius of the crystalsome. ε can therefore be estimated as 4.7% and 11.9% for CS-316 and CS-196, respectively. As κ increases, greater splaying is necessary for the crystal to accommodate the curved surface, which both decreases the crystallinity and increases the inter-stem distance (hence d-spacing). From this observation, we can also conclude that the obvious d-spacing change is seen only in the smallest crystalsome, where significant lattice strain exists (11.9%).

3) ***Curvature dependent CTE***. *In-situ* WAXD data also showed a curvature dependent CTE behavior. Thermal expansion of the (110)/(200) reflection peaks for all three samples show a transition at 144 °C, with both the FSC and CS-316 decrease from 6.8 x 10^{-4} Å/°C to 4.6 x 10^{-4} Å/°C and from 7.8 x 10^{-4} Å/°C to 5.8 x 10^{-4} Å/°C, respectively, while for CS-196, it increases from 8.0 x 10^{-4} Å/ °C to 1.5 x 10^{-3} Å/ °C and then decreases to 9.9 x 10^{-4} Å/ °C upon further heating. The interesting curvature dependent CTE is likely due to the geometrical and structural differences between crystalsomes and FSCs. The sudden change of CTE at 144 °C can be attributed to the melting/re-crystallization processes. For FSC and large crystalsomes, the gained mobility of the local chains at 144 °C leads to rearrangement/melting of defect-rich domains and relaxation of small crystallites, and therefore slightly decreased CTE. However, for the small crystalsome such as CS-196, the crystallites are tightly packed with larger lattice strain, and there is also significant compression on the inner part of the lattice (self-confinement). Because of this, at 144 °C, the gained mobility releases the strain and compression on the inner part of the shell by collectively expanding of the crystalsome. Once the stress is relieved sufficiently the CTE decreases again at the onset of the main melting peak.

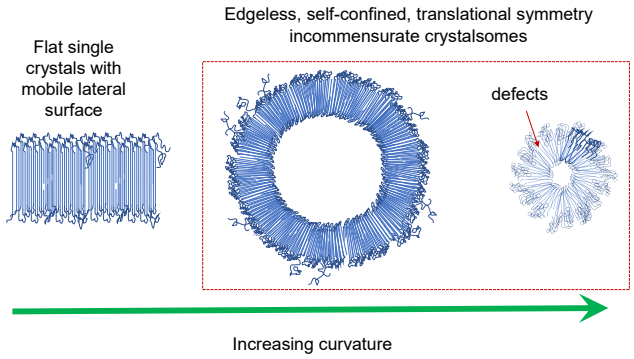

Figure 4. Schematics of FSCs and crystalsomes. In the edgeless and self-confined crystalsomes, tangential expansion can only be accommodated to a limited degree by defect rearrangement. With increasing curvature from left to right, crystals show lower crystallinity, higher disorder, stronger confinement, and more hindered relaxation upon melting.

4) ***Curvature dependent crystallite size***. WAXD results demonstrated that the crystallite size or coherence length of the crystalsome are curvature dependent. CS-196 has a significantly smaller crystallite size compared with larger crystalsomes and FSCs, and the crystallite size is also less sensitive to temperature. Upon heating, for FSC and CS-316, the crystallite size gradually increases followed by a rapid increase at

the onset of melting and then decreases through the melting region. The gradual increase of the crystallite size can be attributed to the annealing effect upon heating, which induces larger coherence length in the crystal. At the onset of melting, as previously discussed, chains become more mobile and the annealing process becomes more efficient, leading to more rapidly increased crystallite size. At a further increased temperature, a moderate portion of the crystals are molten, leading to the decreased crystallite size. Note that the temperature dependency of the crystallite size for FSC and CS-316 are qualitatively similar while the rapid increase/decrease region upshifted for CS-316. This again is attributed to the crystalsome being edgeless and self-confined, so that significant local chain re-arrangement is achieved at a higher temperature for CS-316 compared with FSCs. When curvature is further increased as in the case of CS-196, the chains are more tightly packed with greater stiffness of the crystalsome,[11] and local chain rearrangement becomes more difficult (stronger confinement effect). Furthermore, the high curvature is incommensurate with translation symmetry and large coherence length. The crystallite size therefore maintained largely the same before it suddenly dropped upon crystal melting. This observation is consistent with the temperature dependent CTE behavior.

In summary, we presented in this work the melting behavior of edgeless PLLA crystalsomes and FSCs. The crystallinity, (*hk0*) d-spacing, CTE, and crystallite size of crystalsomes and their temperature dependency are curvature dependent, and are significantly different from conventional FSCs. With increasing curvature, we observed lower crystallinity, higher disorder, stronger confinement effect, and more hindered relaxation upon melting. These behaviors were attributed to the crystalsomes being edgeless, self-confined, and incommensurate with translational symmetry.

ASSOCIATED CONTENT

Supporting Information

The Supporting Information is available free of charge on the ACS Publications website at DOI: Experimental details, crystallization temperature program, dynamic light scattering results, and an AFM image of PLLA FSCs.

AUTHOR INFORMATION

Corresponding Author

* Christopher Li, E-mail: chrisli@drexel.edu
ORCID ID: 0000-0003-2431-7099

Author Contributions

MS conducted the experiments and data analysis. RL and MF assisted with the X-ray experiments. CL directed the project. The manuscript was written through contributions of all authors.

Notes

The authors declare no competing financial interest.

ACKNOWLEDGMENT

This research was financially supported by the National Science Foundation DMR 1709136. This research used the Complex Materials Scattering (CMS/11-BM) beamline, operated by the National Synchrotron Light Source II at Brookhaven National Laboratory, which is supported by the U.S. Department of Energy, Office of Science, Office of Basic Energy Sciences, under Contract DE-SC0012704.

REFERENCES

1. Wunderlich, B., *Macromolecular physics vol. 1: Crystal structure, morphology, defects*. Academic Press: New York, 1973.
2. Geil, P., *Polymer single crystals*. Wiley-Interscience: 1963.
3. Hoffman, J. D.; Davis, G. T.; Lauritzen, J. I., The rate of crystallization of linear polymers with chain folding. In *Treatise on solid state chemistry*, Springer: 1976; pp 497-614.
4. Wunderlich, B., *Macromolecular physics vol 3: Crystal melting*. Academic Press: New York, 1980.
5. Keller, A.; Cheng, S. Z. D., The role of metastability in polymer phase transitions. *Polymer* **1998,** *39*, 4461-4487.
6. Organ, S. J.; Hobbs, J. K.; Miles, M. J., Reorganization and melting of polyethylene single crystals: Complementary tem, dsc, and real-time afm studies. *Macromolecules* **2004,** *37*, 4562-4572.
7. Keller, A., Polymer crystals. *Rep. Prog. Phys.* **1968,** *31*, 623.
8. Zhu, D.-S.; Liu, Y.-X.; Shi, A.-C.; Chen, E.-Q., Morphology evolution in superheated crystal monolayer of low molecular weight poly (ethylene oxide) on mica surface. *Polymer* **2006,** *47*, 5239-5242.
9. Chai, L.; Liu, X.; Sun, X.; Li, L.; Yan, S., In situ observation of the melting behaviour of peo single crystals on a pvph substrate by afm. *Polym. Chem.* **2016,** *7*, 1892-1898.
10. Fujita, M.; Doi, Y., Annealing and melting behavior of poly(l-lactic acid) single crystals as revealed by in situ atomic force microscopy. *Biomacromolecules* **2003,** *4*, 1301-1307.
11. Wang, W.; Qi, H.; Zhou, T.; Mei, S.; Han, L.; Higuchi, T.; Jinnai, H.; Li, C. Y., Highly robust crystalsome via directed polymer crystallization at curved liquid/liquid interface. *Nat. Commun.* **2016,** *7*, 10599.
12. Wang, W.; Staub, M. C.; Zhou, T.; Smith, D. M.; Qi, H.; Laird, E. D.; Cheng, S.; Li, C. Y., Polyethylene nano crystalsomes formed at a curved liquid/liquid interface. *Nanoscale* **2018,** *10*, 268-276.
13. Qi, H.; Zhou, H.; Tang, Q.; Lee, J. Y.; Fan, Z.; Kim, S.; Staub, M. C.; Zhou, T.; Mei, S.; Han, L.; Pochan, D. J.; Cheng, H.; Hu, W.; Li, C. Y., Block copolymer crystalsomes with an ultrathin shell to extend blood circulation time. *Nat. Commun.* **2018,** *9*, 3005.
14. Qi, H.; Liu, X.; Henn, D. M.; Mei, S.; Staub, M. C.; Zhao, B.; Li, C. Y., Breaking translational symmetry via polymer chain overcrowding in molecular bottlebrush crystallization. *Nat. Commun.* **2020,** *11*, 2152.
15. Staub, M. C.; Li, C. Y., Confined and directed polymer crystallization at curved liquid/liquid interface. *Macromol. Chem. Phys.* **2018,** *219*, 1700455.
16. Staub, M. C.; Li, C. Y., Polymer crystallization at liquid-liquid interface. *Polymer Crystallization* **2018,** *1*, 10045.
17. Staub, M. C.; Li, C. Y., Towards shape-translational symmetry incommensurate polymer crystals. *Polymer* **2020**, 122407.
18. Keith, H.; Padden, F., Banding in polyethylene and other spherulites. *Macromolecules* **1996,** *29*, 7776-7786.
19. Li, C. Y.; Cheng, S. Z. D.; Ge, J. J.; Bai, F.; Zhang, J. Z.; Mann, I. K.; Harris, F. W.; Chien, L. C.; Yan, D. H.; He, T. B.; Lotz, B., Double twist in helical polymer "soft" crystals. *Phys. Rev. Lett.* **1999,** *83*, 4558-4561.
20. Cai, W.; Li, C. Y.; Li, L.; Lotz, B.; Keating, M.; Marks, D., Sub-micro tube/scroll polymer single crystal from nylon 6,6. *Adv. Mater.* **2004,** *16*, 600-605.
21. Burks, G. R.; Qi, H.; Gleeson, S. E.; Mei, S.; Li, C. Y., Structure and morphology of poly (vinylidene fluoride) nanoscrolls. *ACS Macro Lett.* **2017,** *7*, 75-79.
22. Wen, T.; Sun, H.-J.; Lotz, B.; Cheng, S. Z., Scrolled/cylindrical solution-grown single crystals in form iii of isotactic poly (1-butene). *Macromolecules* **2020**.
23. Xiong, H.; Chen, C.-K.; Lee, K.; Van Horn, R. M.; Liu, Z.; Ren, B.; Quirk, R. P.; Thomas, E. L.; Lotz, B.; Ho, R.-M., Scrolled polymer single crystals driven by unbalanced surface stresses: Rational design and experimental evidence. *Macromolecules* **2011,** *44*, 7758-7766.

24. Castro-Aguirre, E.; Iniguez-Franco, F.; Samsudin, H.; Fang, X.; Auras, R., Poly (lactic acid)—mass production, processing, industrial applications, and end of life. *Adv. Drug Del. Rev.* **2016,** *107*, 333-366.
25. Di Lorenzo, M. L.; Androsch, R., *Synthesis, structure and properties of poly (lactic acid)*. Springer: 2018.
26. Di Lorenzo, M. L., Calorimetric analysis of the multiple melting behavior of poly(l-lactic acid). *J. Appl. Polym. Sci.* **2006,** *100*, 3145-3151.
27. Gracia-Fernández, C. A.; Gómez-Barreiro, S.; López-Beceiro, J.; Naya, S.; Artiaga, R., New approach to the double melting peak of poly(l-lactic acid) observed by dsc. *J. Mater. Res.* **2012,** *27*, 1379-1382.
28. Yasuniwa, M.; Tsubakihara, S.; Sugimoto, Y.; Nakafuku, C., Thermal analysis of the double-melting behavior of poly(l-lactic acid). *J. Polym. Sci. Polym. Phys.* **2004,** *42*, 25-32.
29. Kalish, J. P.; Aou, K.; Yang, X.; Hsu, S. L., Spectroscopic and thermal analyses of α′ and α crystalline forms of poly(l-lactic acid). *Polymer* **2011,** *52*, 814-821.
30. Kalish, J. P.; Zeng, X.; Yang, X.; Hsu, S. L., A spectroscopic analysis of conformational distortion in the α′ phase of poly(lactic acid). *Polymer* **2011,** *52*, 3431-3436.
31. Zhang, J.; Duan, Y.; Sato, H.; Tsuji, H.; Noda, I.; Yan, S.; Ozaki, Y., Crystal modifications and thermal behavior of poly(l-lactic acid) revealed by infrared spectroscopy. *Macromolecules* **2005,** *38*, 8012-8021.
32. Kawai, T.; Rahman, N.; Matsuba, G.; Nishida, K.; Kanaya, T.; Nakano, M.; Okamoto, H.; Kawada, J.; Usuki, A.; Honma, N.; Nakajima, K.; Matsuda, M., Crystallization and melting behavior of poly (l-lactic acid). *Macromolecules* **2007,** *40*, 9463-9469.
33. Pan, P.; Yang, J.; Shan, G.; Bao, Y.; Weng, Z.; Cao, A.; Yazawa, K.; Inoue, Y., Temperature-variable ftir and solid-state 13c nmr investigations on crystalline structure and molecular dynamics of polymorphic poly(l-lactide) and poly(l-lactide)/poly(d-lactide) stereocomplex. *Macromolecules* **2012,** *45*, 189-197.
34. Lotz, B., Crystal polymorphism and morphology of polylactides. In *Synthesis, structure and properties of poly (lactic acid)*, Springer: 2017; pp 273-302.
35. Liu, G.; Zhang, X.; Wang, D., Tailoring crystallization: Towards high-performance poly (lactic acid). *Adv. Mater.* **2014,** *26*, 6905-6911.
36. Wunderlich, B., *Thermal analysis of polymeric materials*. Springer Science & Business Media: 2005.
37. Strobl, G. R., *The physics of polymers*. Springer: Berlin, 1997.
38. Meng, G.; Paulose, J.; Nelson, D. R.; Manoharan, V. N., Elastic instability of a crystal growing on a curved surface. *Science* **2014,** *343*, 634-637.

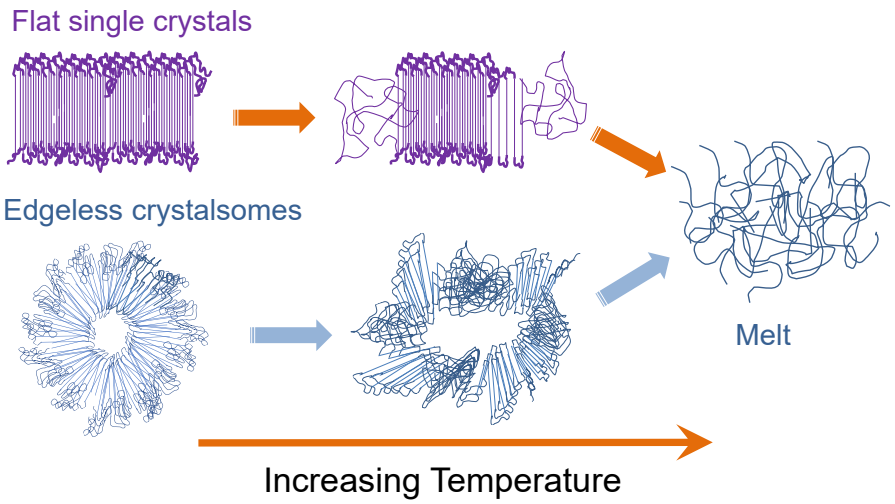
Flat single crystals
Edgeless crystalsomes
Melt
Increasing Temperature